J. Fluid Mech. (1982), *vol.* 117, *pp.* 233–249
Printed in Great Britain

The effects of significant viscosity variation on convective heat transport in water-saturated porous media

By J. GARY,†
Computer Science Department, University of Colorado, Boulder, Colorado 80309, U.S.A.

D. R. KASSOY, H. TADJERAN
Mechanical Engineering Department, University of Colorado, Boulder, Colorado 80309, U.S.A.

AND A. ZEBIB
Mechanical Engineering Department, Rutgers University, Piscataway, New Jersey 08854, U.S.A.

(Received 10 November 1980 and in revised form 1 September 1981)

Weakly nonlinear theory and finite-difference calculations are used to describe steady-state and oscillatory convective heat transport in water-saturated porous media. Two-dimensional rolls in a rectangular region are considered when the imposed temperature difference between the horizontal boundaries is as large as 200 K, corresponding to a viscosity ratio of about 6·5. The lowest-order weakly nonlinear results indicate that the variation of the Nusselt number with the ratio of the actual Rayleigh number to the corresponding critical value R/R_c, is independent of the temperature difference for the range considered. Results for the Nusselt number obtained from finite-difference solutions contain a weak dependence on temperature difference which increases with the magnitude of R/R_c. When $R/R_c = 8$ the constant-viscosity convection pattern is steady, while those with temperature differences of 100 and 200 K are found to oscillate.

1. Introduction

Booker (1976) has reported on measurements of convective heat transfer in a high-Prandtl-number, temperature-dependent-viscosity fluid, polybutene no. 8, confined between horizontal plates. He found that the Nusselt number N declined with an increase in the ratio of the viscosities at the top and bottom boundaries when the viscous-liquid Rayleigh number R_v (defined in (32)), based on the mean value of the viscosity, is fixed. Subsequently, Booker & Stengel (1978) showed that the decrease could be attributed to an increase in the critical Rayleigh number R_{vc} with increasing viscosity ratio. In particular they found that, for $R_v/R_{vc} \gtrsim 10$ and viscosity ratios up to 300, the heat-transfer results could be correlated by $N = 1{\cdot}49(R_v/R_{vc})^{0{\cdot}281}$. A universal curve describes the Nusselt-number variation for the specified range of Rayleigh number and impressed temperature difference.

In this paper we report on a related analogous result, for water-saturated porous

† Present address: Mathematics Department, Colorado School of Mines, Golden, Colorado 80401, U.S.A.

media with large temperature variations, derived from analytical and numerical solution development. We consider two-dimensional convection rolls in a rectangle when the temperature difference between the isothermal horizontal surfaces is as large as 200 K. This maximum viscosity ratio (top to bottom), about 6·5, implies relatively large viscosity variations for this water-based system.† The geometrical configuration mimics the apparatus used by Caltagirone, Clopeau & Combarnous (1971) to observe steady and oscillatory two-dimensional rolls at supercritical Rayleigh numbers. These experiments, carried out in a saturated porous medium 38 cm long, 2 cm wide and between 4 and 6 cm in height, show that a thin vertical slab configuration will suppress three-dimensional modes, even at relatively high Rayleigh numbers. Straus & Schubert (1978) have used stability theory to show that a steady two-dimensional roll in a sufficiently narrow rectangular parallelepiped cannot be destabilized in the third dimension.

An analytical solution, based on weakly nonlinear theory (Palm, Weber & Kvernvold 1972) is developed for the variable-viscosity problem. A related formulation is described by Joseph (1976), although no specific results are given. In our theory the porous medium Rayleigh number R is based on the kinematic-viscosity value at the upper cold boundary. Linear stability theory based on that Rayleigh-number definition (Kassoy & Zebib 1975) shows that the critical value decreases with increasing viscosity ratio (temperature difference) across the system. A two-term expansion for N, when R is close to R_c, is derived for temperature differences up to 200 K. It is observed that N is essentially invariant for constant R/R_c values over the temperature range considered.

Solutions at larger values of R/R_c are obtained by numerical methods (Garg & Kassoy 1981) developed originally for computation of high-Rayleigh-number, constant-viscosity convection in saturated porous media. It is observed that the steady-state Nusselt number at a given value of R/R_c is nearly but not quite invariant to the temperature difference. We find that the difference between the steady Nusselt-number value for the case of constant viscosity (nearly vanishing temperature difference) and that for a 200 K difference is at most about 7 % for the range of R/R_c considered. Although the general effect of temperature difference on steady-state convection is weak, it appears to have a more significant effect on the onset of oscillations in the system. When $R/R_c = 8$, constant-viscosity convection is shown to be steady. In contrast, a regular oscillatory mode exists for $\Delta T^* = 100$ and 200 K.

2. Mathematical system

The geometrical configuration consists of a rectangle of height L^* and width W^*. The horizontal boundaries at $z^* = 0$ and $z^* = -L^*$ are kept at constant temperatures T_0^* and T_1^* respectively, and are assumed impermeable. The vertical boundaries are assumed to be impermeable and thermally insulated. The non-dimensional equations of natural convection can be written in the form

$$\mu\nabla^2\Psi + \mu_x\Psi_x + \mu_z\Psi_z + \theta_x = 0, \tag{1}$$

$$R(\theta_t + \Psi_x + \theta_x\Psi_z - \theta_z\Psi_x) - \nabla^2\theta = 0. \tag{2}$$

† Significantly larger variations are found in various oil-based systems and in the hypothetical models of mantle convection.

The Boussinesq approximation has been invoked, and the liquid specific heat and the medium thermal conductivity are assumed constant. The boundary conditions are

$$\left.\begin{aligned} \theta(x,0,t) = \theta(x,-1,t) = \Psi(x,0,t) = \Psi(x,-1,t) = 0, \\ \theta_x(0,z,t) = \theta_x(A,z,t) = \Psi(0,z,t) = \Psi(A,z,t) = 0. \end{aligned}\right\} \tag{3}$$

The variables in (1)–(3) have been defined with respect to dimensional (starred) quantities by

$$\Psi = \Psi^*/q_r^* L^*, \quad q_r^* = \frac{g^* k^* \alpha^* \Delta T^*}{\nu_0^*},$$

$$\tau = (T_1^* - T_0^*)/T_0^*, \quad \tau\theta = T - (1-\tau z), \quad T = T^*/T_0^*,$$

$$x = x^*/L^*, \quad \mu = \mu^*/\mu_0^*, \quad A = W^*/L^*,$$

$$t = t^*/t_r^*, \quad t_r^* = (\rho^* C^*)_m L^*/q_r^* (\rho^* C^*)_f,$$

$$R = \frac{g^* k^* \alpha^* \Delta T^* L^*}{\nu_0^{*2}} \frac{C_f^* \mu_0^*}{\lambda_m^*}.$$

Here, g^* is the gravity constant, k^* is the permeability, α^* is the thermal-expansion coefficient, $\Delta T^* = T_1^* - T_0^*$, ν_0^* is the kinematic viscosity evaluated at T_0^*, μ_0^* is the viscosity at T_0^*, λ_m^* is the medium thermal conductivity, C_f^* is the liquid specific heat, and C_m^* is the medium specific heat. The quantity $1-\tau z$ represents the rest-state temperature distribution. It should be noted that the porous-medium Rayleigh number R, based on the cold-boundary kinematic viscosity, is to be considered as a 'bookkeeping' value rather than as locally representative. The variation in viscosity across the system implies that the local value of the Rayleigh number near the hot bottom is significantly larger than that near the upper surface. This effect causes the critical value of R for onset of convection to decrease strongly as ΔT^* is increased (Kassoy & Zebib 1975).

The viscosity dependence on temperature of water is described accurately by the empirical curve used by Wooding (1957). In the present notation and with $T_0^* = 298$ K, we can write

$$\mu(z,\theta) = \frac{38}{38 - \Delta T^*(z-\theta)} [1 + a_1 \Delta T^*(z-\theta) - a_2 \Delta T^{*2}(z-\theta)^2], \tag{4}$$

where $a_1 = 3{\cdot}17 \times 10^{-4}$, $a_2 = 2{\cdot}56 \times 10^{-6}$ and ΔT^* is a pure number. This formula, valid to $\Delta T^* \simeq 200$ K, is used in order to model convection phenomena in liquid water specifically. In this sense the results are of interest in the context of geothermal processes in the Earth's crust (Garg & Kassoy 1981).

In the derivation of the mathematical model in (1) and (2) it is assumed that the thermal-expansion coefficient α^* is a constant. In fact for systems with $\Delta T^* = 200$ K and $T_0^* = 298$ K, α^* varies by a factor of nearly 5·5. Straus & Schubert (1977) have included this effect in their definitive study of the linear stability properties of related systems. It should be recognized that the α^* effect on the density is of the magnitude of 10 %. There is then a concomitant effect on the natural convection-driving mechanism. In contrast, the magnitude of the velocity components is inversely proportional to the viscosity for a porous-medium system. It follows that viscosity variations of the magnitude considered here will have a more profound effect on the convective motion than will the variable thermal expansion coefficient. A quantitative estimate of these

effects on linear stability is given by Morland, Zebib & Kassoy (1977). While one may expect similar effects to prevail in the nonlinear regime, a definitive statement requires a more complete model than that used here.

Finally one should note that liquid water has a modest Prandtl number of about 6 at 298 K. At 400 K the value is about 1·4. Further increase in the temperature causes an additional decrease to the neighbourhood of unity (Edwards, Denney & Mills 1979).

3. Finite-amplitude analysis

In weakly nonlinear theory, where the amplitudes of Ψ and θ are finite but small, the viscosity function (4) can be expanded as a Taylor series

$$\mu = f_0(z) + f_1(z)\,\theta + \tfrac{1}{2} f_2(z)\,\theta^2 + \dots . \tag{5}$$

Here

$$f_i(z) = \left.\frac{\partial^i \mu(z,\theta)}{\partial \theta^i}\right|_{\theta=0} \quad (i = 0, 1, 2, \dots).$$

Then in standard fashion (1) and (2) can be arranged in the form

$$\mathbf{L}\boldsymbol{\Phi} = \mathbf{N}, \tag{6}$$

$$\boldsymbol{\Phi} = \begin{bmatrix} \Psi \\ \theta \end{bmatrix}, \quad \mathbf{L} = \begin{bmatrix} f_0\nabla^2 + f_0'\dfrac{\partial}{\partial z} & \dfrac{\partial}{\partial x} \\ -R_c\dfrac{\partial}{\partial x} & \nabla^2 \end{bmatrix}, \tag{7a, b}$$

$$\mathbf{N} = \begin{bmatrix} -(f_1\Psi_z\theta)_z - f_1(\Psi_x\theta)_x - \tfrac{1}{2}(f_2\Psi_z\theta^2)_z - \tfrac{1}{2}f_2(\Psi_x\theta^2)_x \\ R_c(\theta_t + \theta_x\Psi_z - \theta_z\Psi_x) + \Delta R(\theta_t + \Psi_x + \theta_x\Psi_z - \theta_z\Psi_x) \end{bmatrix}, \tag{7c}$$

where primes denote differentiation with respect to z, and $\Delta R = R - R_c$.

The solution to (3), (6) and (7) is assumed to have the form

$$\boldsymbol{\Phi} = \epsilon(t)\,\boldsymbol{\Phi}_1(x,z) + \tilde{\boldsymbol{\Phi}}_1(x,z,t). \tag{8}$$

Here $\epsilon(t)$ is a small amplitude to be found. $\boldsymbol{\Phi}_1(x,z)$, the linear stability analysis neutral mode, satisfies $\mathbf{L}\boldsymbol{\Phi}_1 = 0$. It is given by

$$\boldsymbol{\Phi}_1 = \begin{bmatrix} \Psi_1(z)\sin\alpha x \\ \theta_1(z)\cos\alpha x \end{bmatrix}, \quad \alpha = \frac{\pi}{A}, \tag{9}$$

$$\Psi_1 = \frac{1}{\alpha R_c}(\theta_1'' - \alpha^2\theta_1), \tag{10}$$

$$\left.\begin{aligned} \theta_1^{\mathrm{iv}} + \frac{f_0'}{f_0}\theta_1''' - 2\alpha^2\theta_1'' - \frac{\alpha^2 f_0'}{f_0}\theta_1' + \left(\alpha^4 - \frac{\alpha^2 R_c}{f_0}\right)\theta_1 = 0, \\ \theta_1(0) = \theta_1(-1) = \theta_1''(0) = \theta_1''(-1) = 0. \end{aligned}\right\} \tag{11}$$

Equation (11) is the linear stability eigenvalue problem considered by Kassoy & Zebib (1975). The correction $\tilde{\boldsymbol{\Phi}}_1$ is described by

$$\mathbf{L}\tilde{\boldsymbol{\Phi}}_1 = \begin{bmatrix} d_1 \\ d_2 \end{bmatrix}, \tag{12}$$

where

$$d_1 = \epsilon^2[\alpha^2 f_1 \Psi_1 \theta_1 - \tfrac{1}{2}(f_1 \theta_1 \Psi_1')'] \sin 2\alpha x$$
$$- \tfrac{1}{8}\epsilon^3[(f_2 \theta_1^2 \Psi_1')' + 3\alpha^2 f_2 \Psi_1 \theta_1^2](\sin \alpha x + \sin 3\alpha x),$$
$$d_2 = [\dot{\epsilon} R_c \theta_1 + \epsilon\alpha(\Delta R)\Psi_1] \cos \alpha x - \tfrac{1}{2}\epsilon^2 R_c \alpha(\theta_1 \Psi_1' + \Psi_1 \theta_1')$$
$$+ \tfrac{1}{2}\epsilon^2 R_c \alpha(\theta_1 \Psi_1' - \Psi_1 \theta_1') \cos 2\alpha x,$$

with $\dot{\epsilon} = d\epsilon/dt$. The compatibility condition required for (3) and (12) is found by first defining the adjoint operator $\mathbf{L}^*$ by

$$(\mathbf{LU}, \mathbf{V}) = (\mathbf{U}, \mathbf{L}^*\mathbf{V}),$$

where

$$(\mathbf{LU}, \mathbf{V}) = \int_0^A dx \int_{-1}^0 (\mathbf{LU}) \cdot \mathbf{V}\, dz,$$

and U and V are two vector functions with four continuous derivatives on $0 \leqq x \leqq A$ and $-1 \leqq z \leqq 0$, and satisfying the boundary conditions (3). We find that

$$\mathbf{L}^* = \begin{bmatrix} f_0 \nabla^2 + f_0' \dfrac{\partial}{\partial z} & R_c \dfrac{\partial}{\partial x} \\ -\dfrac{\partial}{\partial x} & \nabla^2 \end{bmatrix}. \tag{13}$$

The solution to

$$\mathbf{L}^* \boldsymbol{\Phi}_1^* = 0$$

and (3) is found to be

$$\boldsymbol{\Phi}_1^* = \begin{bmatrix} R_c \Psi_1 \sin \alpha x \\ \theta_1 \cos \alpha x \end{bmatrix}. \tag{14}$$

The compatibility condition

$$(\mathbf{L}\tilde{\boldsymbol{\Phi}}_1, \boldsymbol{\Phi}_1^*) = 0 \tag{15}$$

can be used in (12) to show that

$$\dot{\epsilon} = O(\epsilon^3), \quad \Delta R = O(\epsilon^2), \tag{16}$$

which means that several contributions to d_1 and d_2 below (12) are superfluous to the order considered. These terms must be carried over to the next-higher-order perturbation equations. It follows that

$$\tilde{\boldsymbol{\Phi}}_1 = \epsilon^2[\boldsymbol{\Phi}_0(z) + \boldsymbol{\Phi}_2(x, z)], \tag{17}$$

where

$$\boldsymbol{\Phi}_0 = \begin{bmatrix} 0 \\ \theta_0(z) \end{bmatrix}, \quad \boldsymbol{\Phi}_2 = \begin{bmatrix} \Psi_2(z) \sin 2\alpha x \\ \theta_2(z) \cos 2\alpha x \end{bmatrix}. \tag{18}$$

The term $\boldsymbol{\Phi}_0(z)$ represents modifications to the basic rest-state due to nonlinear interactions. The stream-function component is zero since there is no net mass flow across the boundaries, while the temperature-perturbation component $\theta_0(z)$ signifies a change (increase) in the net heat transfer across the horizontal boundaries. The functions $\theta_0(z)$, $\Psi_2(z)$ and $\theta_2(z)$ are found by solving the following ordinary differential equations:

$$\theta_0'' = -\tfrac{1}{2}\alpha R_c(\theta_1 \Psi_1' + \Psi_1 \theta_1'), \quad \theta_0(0) = \theta_0(-1) = 0; \tag{19}$$

$$\left.\begin{aligned} f_0(\Psi_2'' - 4\alpha^2 \Psi_2) + f_0' \Psi_2' - 2\alpha\theta_2 &= \alpha^2 f_1 \Psi_1 \theta_1 - \tfrac{1}{2}(f_1 \theta_1 \Psi_1')', \\ -2\alpha R_c \Psi_2 + \theta_2'' - 4\alpha^2 \theta_2 &= \tfrac{1}{2}\alpha R_c(\theta_1 \Psi_1' - \Psi_1 \theta_1'), \\ \theta_2(-1) = \theta_2(0) = \Psi_2(0) &= \Psi_2(-1) = 0. \end{aligned}\right\} \tag{20}$$

The next correction to Φ is found by letting

$$\Phi = \epsilon\Phi_1 + \epsilon^2(\Phi_0 + \Phi_2) + \tilde{\Phi}_2(x, z, t) \tag{21}$$

in (6). This leads to

$$L\tilde{\Phi}_2 = -\begin{bmatrix} \tfrac{1}{8}\epsilon^3[-(f_2\theta_1^2\Psi_1') + 3\alpha^2 f_2\Psi_1\theta_1^2](\sin\alpha x + \sin 3\alpha x) \\ -\epsilon^3[(f_1\theta_0\Psi_1')'\sin\alpha x + \tfrac{1}{2}(f_1\theta_2\Psi_1')'(\sin 3\alpha x - \sin\alpha x) \\ +\tfrac{1}{2}(f_1\theta_1\Psi_2')'(\sin\alpha x + \sin 3\alpha x)] \\ +\alpha^2\epsilon^3 f_1[\theta_0\Psi_1\sin\alpha x + \tfrac{1}{2}(\theta_2\Psi_1 + 2\Psi_2\theta_1)(\sin\alpha x + 3\sin 3\alpha x)] \\ [\dot{\epsilon}R_c\theta_1 + \alpha\epsilon(\Delta R)\Psi_1]\cos\alpha x \\ -\alpha R_c\epsilon^3[\theta_0'\Psi_1\cos\alpha x + \tfrac{1}{2}(2\theta_2\Psi_1 + \theta_1\Psi_2')(\cos\alpha x - \cos 3\alpha x) \\ +\tfrac{1}{2}(2\theta_1'\Psi_2 + \theta_2'\Psi_1)(\cos\alpha x + \cos 3\alpha x)] \end{bmatrix} \tag{22}$$

The compatibility condition (15) requires that $\tilde{\Phi}_2 = O(\epsilon^3)$,

$$\begin{aligned} \epsilon^3\int_{-1}^{0}[R_c\Psi_1\{\tfrac{1}{8}[-(f_2\theta_1^2\Psi_1')' + 3\alpha^2 f_2\Psi_1\theta_1^2] - (f_1\theta_0\Psi_1')' + \tfrac{1}{2}(f_1\theta_2\Psi_1')' \\ -\tfrac{1}{2}(f_1\theta_1\Psi_2')' + \alpha^2 f_1[\theta_0\Psi_1 + \tfrac{1}{2}(\theta_2\Psi_1 + 2\Psi_2\theta_1)]\} \\ -\alpha R_c\theta_1[\theta_0'\Psi_1 + \tfrac{1}{2}(2\theta_2\Psi_1' + \theta_1\Psi_2') + \tfrac{1}{2}(2\theta_1'\Psi_2 + \theta_2'\Psi_1)]]\,dz \\ +R_c\dot{\epsilon}\int_{-1}^{0}\theta_1^2\,dz + \alpha\epsilon(\Delta R)\int_{-1}^{0}\theta_1\Psi_1\,dz = O(\epsilon^5). \end{aligned} \tag{23}$$

Equation (23) determines the unknown amplitude $\epsilon(t)$ to $O(\epsilon^5)$. A steady state is possible if there is a real solution to (23) as $t \to \infty$ (or $\dot{\epsilon} \to 0$).

From (23), the steady-state amplitude ϵ_0 is given by

$$\epsilon_0^2 = -\alpha(\Delta R)\int_{-1}^{0}\Psi_1\theta_1\,dz \Big/ I_1 + O(\epsilon_0^4), \tag{24}$$

where I_1 is the value of the first integral in (23). The Nusselt number is described by

$$\begin{aligned} N &= 1 - \frac{1}{A}\int_0^A \left.\frac{\partial\theta}{\partial z}\right|_{z_0} dx \quad (z_0 = -1, 0) \\ &= 1 - (\epsilon_0^2/A)\int_0^A \left.\frac{d\theta_0}{dz}\right|_{z_0} dx = 1 - \epsilon_0^2\left.\frac{d\theta_0}{dz}\right|_{z_0}. \end{aligned} \tag{25}$$

The derivative in (25) can be obtained from the solution to (19):

$$\theta_0(z) = \tfrac{1}{2}R_c\alpha\left(z\int_{-1}^{0}\theta_1\Psi_1\,d\hat{z} + \int_z^0\theta_1\Psi_1\,d\hat{z}\right), \tag{26}$$

where it should be noted that by using (10) the first integral can be written as

$$\int_{-1}^{0}\theta_1\Psi_1\,d\hat{z} = -\frac{1}{\alpha R_c}\int_{-1}^{0}(\theta_1'^2 + \alpha^2\theta_1^2)\,d\hat{z}. \tag{27}$$

It follows that at the upper surface

$$\left.\frac{d\theta_0}{dz}\right|_0 = -\frac{1}{2}\int_{-1}^{0}(\theta_1'^2 + \alpha^2\theta_1^2)\,d\hat{z}. \tag{28}$$

ΔT^* (°C)	τ	R_c	$k-2$
$\to 0$	$\to 0$	$4\pi^2$	0
20	0·067	31·5	0·0043
40	0·134	26·3	0·0020
100	0·336	17·3	0·0005
120	0·402	15·7	0·0009
200	0·671	11·1	0·0093

TABLE 1. The computed value of the proportionality constant k as a function of overheat ratio τ

The Nusselt number at the upper surface, obtained by combining (24), (25), (27) and (28), can be written as

$$N = 1 + k(\alpha, R_c)\,(\Delta R/R_c), \quad k = \left(\int_{-1}^{0} (\theta_1'^2 + \alpha^2\theta_1^2)\,d\hat{z}\right)^2 \Big/ 2I_1, \tag{29}$$

where I_1 is the first integral in (23).

In order to evaluate (29) one first selects a value of the aspect ratio A and the overheat ratio τ. Then the eigenvalue problem in (11) is solved by a quasilinearization technique, described in Kassoy & Zebib (1975), to obtain R_c and θ_1. Equation (10) is used to find Ψ_1. The integral I_1 depends on the functions θ_0, θ_2 and Ψ_2. The first is obtained from the quadrature form in (26). The latter two quantities are found by an integration of (20).

Calculations were carried out for a square, $A = 1$ ($\alpha = \pi$) and the values of τ shown in table 1. It is observed that the proportionality constant k is essentially invariant over the range of τ considered. The value at $\tau = 0, k = 2$, obtained by purely analytical methods, corresponds to the lowest-order result obtained by Palm *et al.* (1972). The source of the invariance is not obvious. For example, the numerator in the k-definition in (29) depends implicitly on $f_0(z)$, defined below (5), while I_1 has an explicit dependence on $f_1(z)$ and $f_2(z)$. As a result it is not possible by algebraic manipulation to reduce I_1 to a quantity proportional to the numerator. The viscosity formula in (4), from which f_0, f_1 and f_2 are obtained, is empirical in nature and exhibits no obvious special qualities that point toward the invariance property.

The result given by (29) is of course valid only for small values of $\Delta R/R_c$. In principle, additional accuracy could be obtained by higher-order calculations and methods like those used by Palm *et al.* (1972). However, given the availability of highly accurate numerical methods like those used in a previous study of constant-viscosity convection (Gary & Kassoy 1981), it seems more useful to proceed to larger values of R/R_c via numerical solutions.

4. The numerical method

The numerical method used to obtain the Nusselt number is described in Gary & Kassoy (1981) and Gary (1981). The system in (1) and (2) is used in the form

$$(\mu\Psi_x)_x + (\mu\Psi_y)_y = -\theta_x, \tag{30}$$

$$\theta_t = \frac{1}{R}(\theta_{xx} + \theta_{yy}) - \Psi_x - \theta_x\Psi_t + \theta_t\Psi_x. \tag{31}$$

	N		
R/R_c	$\Delta T^* = 0$	$\Delta T^* = 100$ K	$\Delta T^* = 200$ K
2	2·2555	2·1691	2·1670
3	2·9355	2·836	2·7761
4	3·4902	3·2875	3·2037
6	4·1191	3·9478	3·8375
8	4·6499	oscillatory	oscillatory

TABLE 2. Average Nusselt number N versus R/R_c for several ΔT^* (K) obtained from a second-order method on a 33×33 grid

The viscosity μ is temperature-dependent. In the computations described in Gary & Kassoy (1981) we assumed a constant viscosity. The only change required for the present work is the use of a more general method to solve the elliptic equation for the stream function $\Psi(x, z, t)$. We had used a direct method, based on a subroutine package by Swarztrauber & Sweet (1975), which does not apply to the variable-viscosity problem. In this work we use the multigrid iterative method to solve the equation for the stream function (Brandt 1977). In most of our runs we used the 'cycling' version of the multigrid algorithm rather than the 'FAS' version. The multigrid method is based on a series of mesh refinements, each with one-half the resolution of the previous mesh. Our cycling version proceeds from the fine mesh down to the lowest-level mesh and back to the fine mesh. Gauss–Seidel 'smoothing' iterations are used on each mesh to reduce the 'high-wavenumber' error on that mesh. We refer to Brandt (1977) for a complete description. This method worked very well for the steady-state solutions that are of concern here. For time-dependent solutions the FAS version would be more efficient. This version starts on the coarse mesh and works up to the fine mesh.

We used the fourth-order ADI (alternating-direction-implicit) method to solve the time-dependent θ-equation. This is described in our previous paper. Generally a time step of $\Delta t = 1{\cdot}0$ (in dimensionless units) was used, since we were looking for a steady-state solution. We reduced the time step to 0·05 or 0·1 for a few cases to verify that the solution is independent of the time step.

The basic five-point difference approximation used to solve for the stream function provides second-order accuracy. An option in our code allows us to obtain a fourth-order accurate solution based on the iterative-improvement idea of Lindberg (1976). This approximately doubles the computing time for the stream function. It requires the computation of a correction term based on fourth-order five-point difference approximations in each co-ordinate direction followed by a second solution of the usual five-point difference approximation using the multigrid subroutine. This will be described in more detail in a forthcoming paper.

The second-order scheme on a 33×33 mesh provides adequate resolution for the steady-state solutions. We have made sufficient runs with second- and fourth-order schemes using 33×33 and 49×49 meshes respectively to ensure the existence of oscillatory solutions at the higher Rayleigh numbers. However, further investigation is required to estimate the precise error in the oscillatory solutions. Detailed consideration of these matters is given in Gary & Kassoy (1981).

	N		
R/R_c	$\Delta T^* = 0$	$\Delta T^* = 100$ K	$\Delta T^* = 200$ K
4	no calculation made	3·2818	3·2021
6	4·1012	3·9348	3·8367

TABLE 3. Average Nusselt number N versus R/R_c for several ΔT^* (K) obtained from a fourth-order method on a 49 × 49 grid

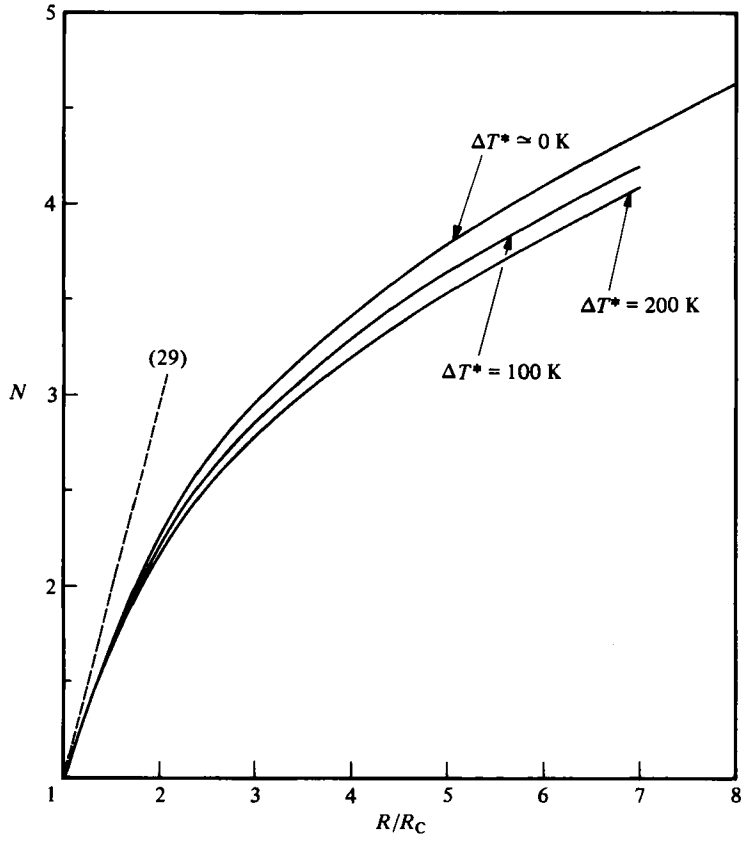

FIGURE 1. The Nusselt-number dependence on the Rayleigh-number ratio for values of the temperature difference ΔT^*. The dashed line, obtained from (29), is the weakly nonlinear result.

5. The numerical results

Specific numerical results were obtained for values of ΔT^* equal to 0, 100 and 200 K for a square with an upper surface temperature at 298 K. In table 2 we show the value of the Nusselt number N, calculated as an integral average of the values found on each horizontal row of grid points including the upper and lower boundaries, for values of R/R_c ranging from 2 to 8. These results were obtained from the second-order scheme on a 33 × 33 mesh. At $R/R_c = 2$ the value of N changes from 2·2555 for the constant-viscosity case ($\Delta T^* = 0$) to 2·1670 when $\Delta T^* = 200$ K, amounting to a

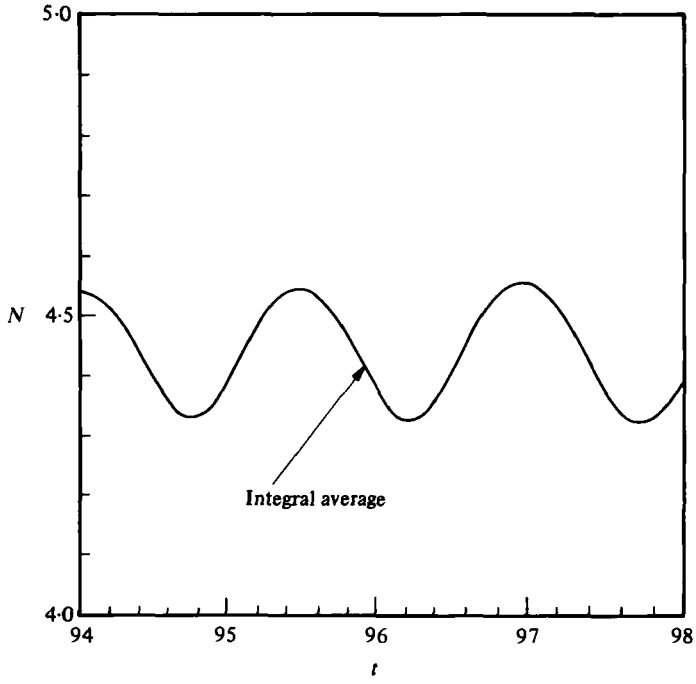

FIGURE 2. The integral average Nusselt number as a function of time for $R/R_c = 8$ and $\Delta T = 200$ K.

3·92 % decrease. At $R/R_c = 6$ the analogous variation is 6·83 %. In order to determine whether these small, but systematic, variations in N with ΔT^* were real, we obtained solutions from a fourth-order scheme on a 49×49 mesh. The results for $R/R_c = 4$ and 6 are shown in table 3. A comparison of the appropriate entries in tables 2 and 3 shows that the variation associated with accuracy level and resolution is at most 0·43 %. This change is an order of magnitude smaller than that associated with the ΔT^* effect. It seems reasonable to conclude that the Nusselt number is weakly dependent on the value of the temperature difference. The dependence increases with R/R_c. Steady-state results, including the weakly nonlinear analytical prediction, are shown in figure 1.

At a fixed value of R/R_c the Nusselt number is observed to decrease slightly as ΔT^* increases. It should be noted that the absolute value of R decreases significantly with the increase in ΔT^*, owing to the associated rapid decline of R_c seen in table 1 (Kassoy & Zebib 1975). In this sense R itself is not a good correlation parameter. It is the use of R/R_c, which evidently compensates for most of the viscosity effects on stability, that leads to a near invariance of N to ΔT^*.

At $R/R_c = 8$ we found a steady-state solution for the constant-viscosity case, $\Delta T^* = 0$, with $N = 4{\cdot}6499$. In contrast, the second-order scheme with 33×33 resolution produced oscillatory solutions at the larger values of ΔT^*. In order to be certain that the unsteadiness was not a numerical fiction, additional computations were carried out using the more accurate fourth-order scheme. We verified the steady result for $\Delta T^* = 0$ and found nearly identical oscillatory results at the larger overheat values. We conclude that the onset of the oscillatory mode is associated with both the

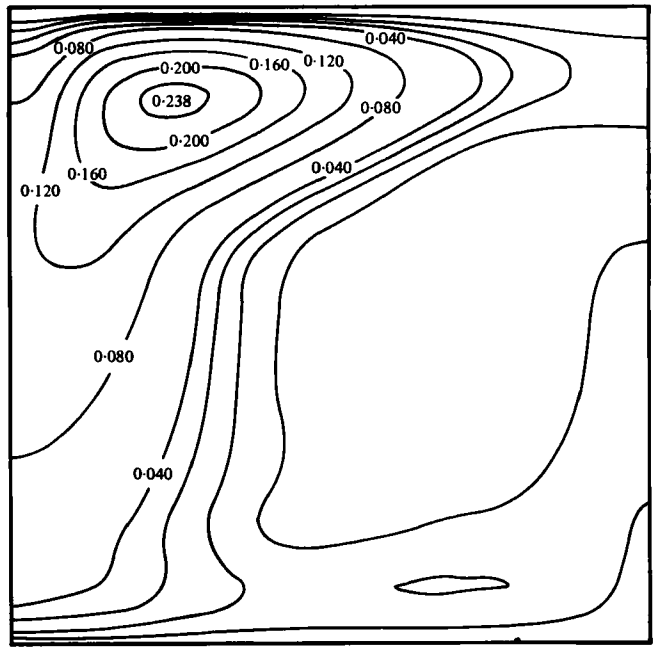

FIGURE 3. Contours of $\theta_{max}-\theta_{min}$ at each grid point obtained from a search over 5 time units for $R/R_c = 8$ and $\Delta T = 200$ K. The contour interval is 0·01 after the 0·04 contour.

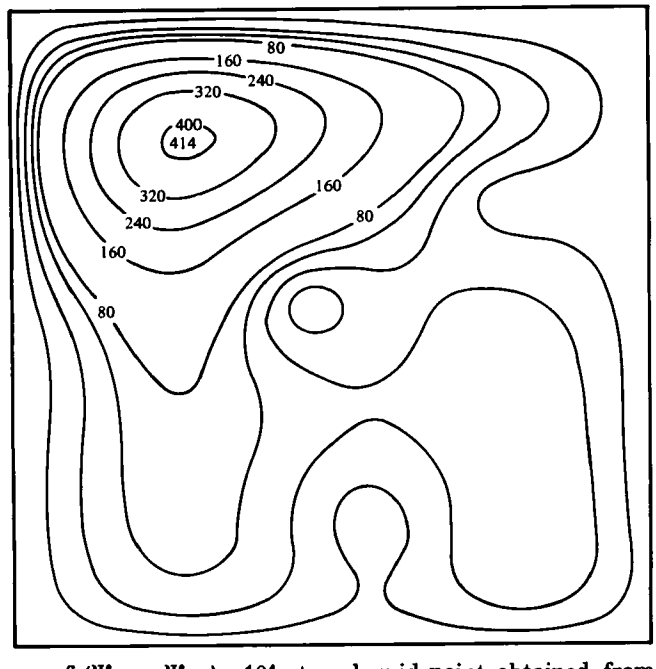

FIGURE 4. Contours of $(\Psi_{max}-\Psi_{min})\times 10^4$ at each grid point obtained from a search over 5 time units for $R/R_c = 8$ and $\Delta T = 200$ K. The contour interval is 20 after the 80 contour.

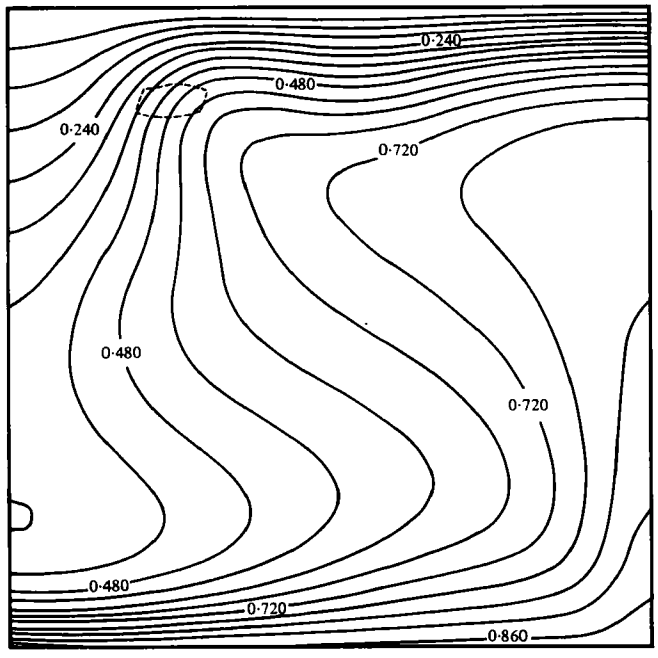

FIGURE 5. Instantaneous isotherms for $(T-1)/\tau$ at $t = 98$ when $R/R_c = 8$ and $\Delta T = 200$ K. The dashed line is the maximum-disturbance contour from figure 3.

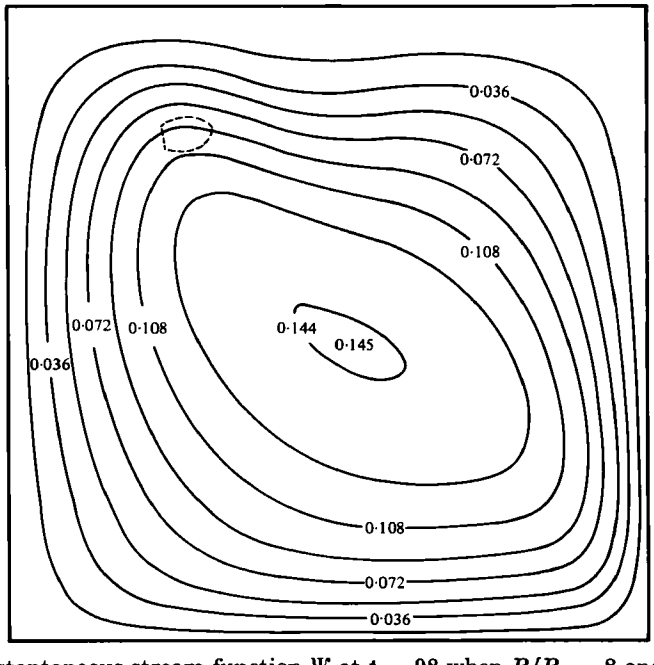

FIGURE 6. Instantaneous stream function Ψ at $t = 98$ when $R/R_c = 8$ and $\Delta T = 200$ K. The dashed line is the maximum-disturbance contour from figure 4.

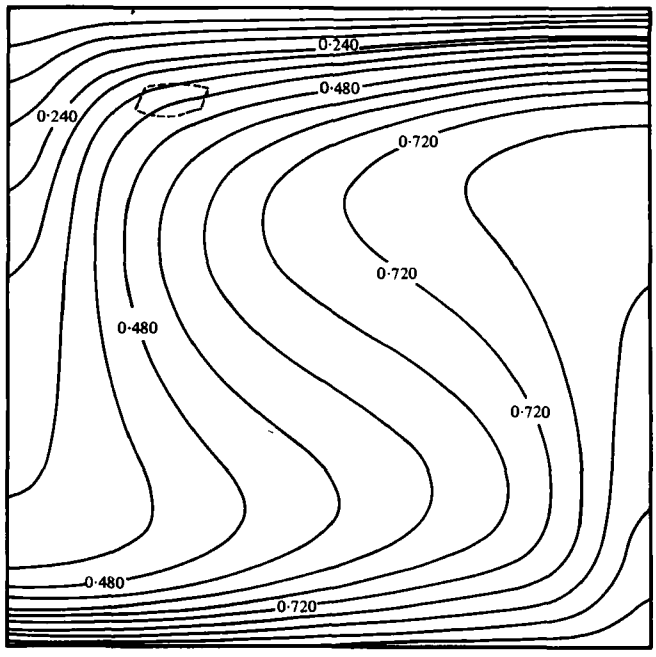

FIGURE 7. Averaged isotherms for $(T-1)/\tau$ obtained over 5 time units when $R/R_c = 8$ and $\Delta T = 200$ K. The dashed line is the maximum-disturbance contour from figure 3.

Rayleigh-number level relative to the critical value and the magnitude of overheat. The latter generates a material-property effect associated with the strong decrease of water viscosity with increasing temperature. It should be noted that Gary & Kassoy (1981) have compared solutions generated with second- and fourth-order methods and resolutions up to a 49×49 grid to show that it is the order of accuracy which is the key to producing a useful description of oscillatory convection. While resolution is important it is apparent for the R/R_c ratios considered here that a 33×33 grid will resolve the spatial structure. Computations on a 49×49 grid were, in our judgement, prohibitively expensive for the improvement obtained.

The oscillating Nusselt number for $R/R_c = 8$ and $\Delta T^* = 200$ K, obtained from a fourth-order calculation on a 33×33 grid, is shown in figure 2 for time units between 94 and 98. A repeatable oscillation amplitude of about 0·2 units occurs with a period of about 1·5 for the interval shown and beyond. The amplitude is similar in size to that observed in extensive calculations for constant-viscosity convection when $R/R_c = 10$, described in Gary & Kassoy (1981). However, the present period is considerably shorter than that observed earlier. The basic character of the oscillation can be ascertained from figures 3 and 4 where we have shown contours of $\theta_{max} - \theta_{min}$ and $\Psi_{max} - \Psi_{min}$ obtained at each grid point, over the five time units prior to 98, corresponding to more than three cycles. One observes that in both cases the oscillation is confined primarily to the upper left-hand corner. One may note the complete lack of variation in the lower right-hand corner where hot, low-viscosity liquid rises from the lower boundary (see figures 5–8). This behaviour is in distinct contrast to that observed for the constant-viscosity flow at $R/R_c = 10$ described in Gary & Kassoy (1981). There, symmetry conditions required equal localized oscillations in the upper left- and lower right-hand

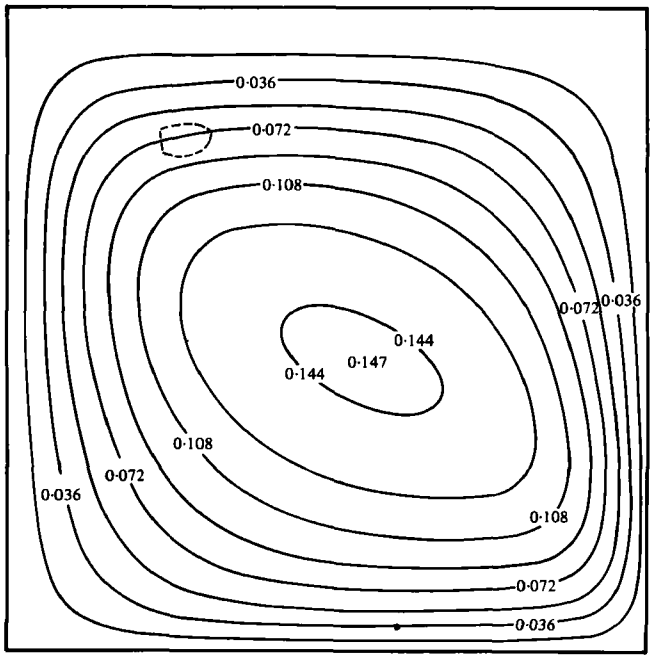

FIGURE 8. Averaged stream function obtained over 5 time units when $R/R_0 = 8$ and $\Delta T = 200$ K. The dashed line is the maximum-disturbance contour from figure 4.

corners. The core region was nearly steady in appearance. It appears that the variable viscosity effect on the oscillatory flow configuration is dramatic. Beginning in the lower right-hand corner of figures 3–8 we observe first the vertical rise of the relatively high speed convection plume of hot, low-viscosity liquid. The dominance of convective heat transport relative to conductive cooling leads to a relatively small vertical temperature gradient. The temperature difference $(T-1)/\tau$ decreases by only 28 % over 86 % of the cell height. Thereafter the temperature gradients are more significant as the effect of the cold upper surface becomes pronounced. When the convecting fluid turns leftward, as portrayed in figures 5 and 7, a well-defined flow of hot liquid penetrates the interior of the system below the cooled surface layer. This flow causes the mushroom-shaped isotherms distorted to the left in the upper half of figures 5 and 7. The horizontal gradient associated with the flow is minimal until we reach the location of the oscillatory maximum seen in figures 3 and 4 and reproduced in figures 5–8. It appears reasonable to surmise that in this vicinity a localized instability develops owing to the interaction between a cool, heavy, near-surface layer and the hot, light liquid just below. A comparison of figures 5 and 7 or figures 6 and 8 shows that there is upward penetration of the hot flow in the instability region for the instantaneous configuration relative to the average system.

The downward convection plume of cooled surface-layer liquid moves more slowly than its hot counterpart. This relatively sluggish response is caused by a characteristic viscosity six times larger than that in the lower right-hand corner, for this system with $\Delta T^* = 200$ K and $T_0^* = 298$ K. Conductive effects are more pronounced, leading to larger vertical temperature gradients than in the hot plume, because the residence time is considerably larger. When the downflowing fluid turns to the right a cool

tongue of liquid penetrates the interior of the cell above a heated bottom boundary layer. It may be observed from figures 5 and 7 that the penetration is considerably less significant than that associated with the hot tongue. For example, in the former drawing we see that, halfway across the cell, the hot leftward-moving tongue has been cooled by about 30 %. In contrast the cold, rightward-moving liquid has been heated by more than 50 %. One may surmise that the instability is absent in the lower right-hand corner because the localized density contrast is much smaller than that in the upper left-hand corner. Certainly, one may note from figure 5 that the change in temperature gradient across the dashed maximum-disturbance contour is significantly different from that seen in the analogous portion of the lower right-hand corner.

6. Discussion

Booker's original data (1976) showed that at a fixed value of the viscous-liquid Rayleigh number, defined by

$$R_{\mathrm{v}} = \alpha^* g^* \Delta T^* L^{*3} / \kappa^* \nu_{\mathrm{A}}^*, \tag{32}$$

where κ^* is the thermal diffusivity and ν_{A}^* is the kinematic viscosity evaluated at the mean of the boundary temperatures, the Nusselt number N declined with an increase in the ratio of the viscosities of the top and bottom boundaries. Booker & Stengel (1978) were then able to show that all the data points were correlated to within 1 % by

$$N = 1{\cdot}49(R_{\mathrm{v}}/R_{\mathrm{vc}})^{0{\cdot}281} \quad (10 \leqslant R_{\mathrm{v}}/R_{\mathrm{vc}} \leqslant 220). \tag{33}$$

The ratio of boundary viscosities was as much as 300 in the high-Prandtl-number liquid used. It should also be noted that the convection modes observed by Booker (1976) in a cylindrical vessel were far more general than the two-dimensional rolls considered in the present porous-media problem.

The results in figure 1 and table 1 may be used to construct a graph of $N = N(R)$. We find that at a given value of R the Nusselt number increases monotonically with ΔT^*. This is physically plausible in our system where the upper boundary temperature is fixed. An increase in ΔT^* means an increase in the bottom-boundary temperature and a reduction in the viscosity in the lower portion of the system leading to enhanced convection. The result is opposite to that found by Booker (1976). There are several possible reasons for the difference. The modes of convection observed by Booker, as well as the container and working fluid, are rather different from those considered here. In general, our R/R_{c} ratios are much smaller than those considered in the pure-fluid experiment. This may be relevant because Torrance & Turcotte (1971) found reduced heat transport with increasing viscosity ratio for computed two-dimensional rolls in a pure fluid with free horizontal boundaries. A more likely explanation can be developed by recognizing that if the bottom temperature of a system is fixed and the top temperature is lowered, then the viscosity ratio will increase but the system will become relatively more viscous and hence less convective in nature. Then the observed decline of the Nusselt number with increasing viscosity ratio is physically plausible in that case. If Booker's (1976) experiment was run by reducing the upper-boundary temperature relative to the lower value then his observation is understandable. Unfortunately there is no detailed description of procedure in the paper.

The success of (33) in predicting the Nusselt number for an extensive range of

conditions motivated us to consider a similar correlation for the present problem. In order to follow the Booker–Stengel approach the porous-medium Rayleigh number, defined below (3), is rewritten as

$$R = g^* k^* \alpha^* \Delta T^* L^* / \nu_0^* \kappa_m^*, \quad \kappa_m^* = \lambda_m^* / \rho_0^* C_f^*, \tag{34}$$

where $k^* L^*$ plays the role of L^{*3} in (32). If the system properties, g^*, k^*, α^*, L^*, κ_m^* and the upper-boundary temperature T_0^* are specified, then ν_0^* is known. It follows that the Rayleigh number can be written formally as $R = \Omega \Delta T^*$ where the known value of Ω can be found from (34). In this sense

$$R/R_c = \Delta T^*/\Delta T_c^*, \tag{35}$$

where ΔT_c^* is the temperature difference just required for the onset of convection. It follows that figure 1 can be reinterpreted in terms of N as a function of $\Delta T/\Delta T^*$. Similarly one can define a Rayleigh number based on the mean value of the kinematic viscosity:

$$\left.\begin{aligned} R_A &= g^* k^* \alpha^* \Delta T^* L^* / \nu_A^* \kappa_m^* = R(\nu_A^*/\nu_0^*)^{-1}, \\ \nu_A^* &= \tfrac{1}{2}\nu_0^* \left(1 + \frac{\nu_b^*}{\nu_0^*}\right), \end{aligned}\right\} \tag{36}$$

where ν_b^* is the bottom-boundary value of ν^*. It follows that

$$\frac{R_A}{R_{Ac}} = \frac{R}{R_c} \frac{1 + (\nu_{bc}^*/\nu_0^*)}{1 + (\nu_b^*/\nu_0^*)} \gtrsim \frac{R}{R_c}, \tag{37}$$

where the subscript c denotes the critical value. The inequality follows from $\nu_b^* \leqslant \nu_{bc}^*$ for $\Delta T^* \geqslant 0$. If (4) and $\mu^* = \rho^* \nu^*$ are used one may find the explicit dependence of the viscosity term in (36) on ΔT^* and R/R_c.

One may now construct $N = N(R_A)$ from figure 1, table 1 and (36). We find again that there is an increase in N with ΔT^*, although the variation is considerably reduced when compared with that found from $N = N(R)$.

If the sought-after correlation formula is to exist then one should find a single value of N at a specified R_A/R_{Ac} for a range of ΔT^*. Referring to figure 1 we can observe that a constant value of N is found for increasing values of ΔT^* as R/R_c increases. Then in order for the correlation to work it is necessary that $(R_A/R_{Ac}) \lesssim R/R_c$ at a given ΔT^*. Unfortunately (36) shows the opposite to be true. The Booker–Stengel type of correlation does not appear to be valid in this system where increasing viscosity ratio is associated with a less-viscous, more-convective flow process. It is possible however that a more general development might produce a better result. For example the derivation of (37) requires that α^* and κ_m^* are both independent of ΔT^*. Neither condition is physically viable for a water-saturated porous medium.

Although theoretical considerations and the appearance of oscillatory convection limit our study to a range of values of R/R_c far smaller than those considered by Booker & Stengel, it is apparent that the basic conclusions are similar although not identical. Whether in water-saturated porous media or in a pure viscous fluid, the Nusselt number is primarily dependent on the ratio R/R_c. The weak dependence on the bottom-to-top temperature (or viscosity) ratio, found in our numerical calculations, appears to decrease as $R \to R_c$, and vanishes altogether in a first-order weakly nonlinear

theory. It is plausible, but by no means certain, that a weak temperature effect in the pure viscous fluid data is masked by experimental error.

We observed the appearance of a verifiable oscillatory flow at $R/R_c = 8$ when $\Delta T^* = 200$ K, whereas steady flow occurs in the constant-viscosity case. This suggests once again that the physical properties of these rolls are not purely dependent on R/R_c. The oscillatory pattern of the flow differs in a distinct manner from that observed in a constant-viscosity fluid. The most notable difference is associated with the localized instability zone in the region where the cooled surface layer turns downward. The physical origin of the onset of the oscillatory motion and modelling of the process deserve further attention.

The earliest phases of this work were supported by a National Science Foundation Grant, AER 74-03429 A01. Four years later a correction was made in the original non-linear analysis, and extensive new numerical calculations, supported by a National Science Foundation Grant, ENG-77-26893, were carried out. Additional support for two of the authors (D. R. Kassoy and H. Tadjeran) from the U.S. Geological Survey, from 14-08-0001-G-628 and from the National Science Foundation Grant DME 8011730 is gratefully acknowledged.

REFERENCES

Booker, J. R. 1976 *J. Fluid Mech.* **76**, 741.

Booker, J. R. & Stengel, K. C. 1978 *J. Fluid Mech.* **86**, 289.

Brandt, A. 1977 *Math. Comp.* **31**, 333.

Caltagirone, J. P., Cloupeau, M. & Combarnous, M. A. 1971 *C.R. Acad. Sci. Paris* B **273**, 833.

Edwards, D. K., Denney, V. E. & Mills, A. F. 1979 *Transfer Processes.* McGraw-Hill.

Garg, S. K. & Kassoy, D. R. 1981 In *Geothermal Systems: Principles and Case Histories* (ed. L. Rybach & L. J. P. Muffler). Wiley. 37–68.

Gary, J. 1981 On higher order multigrid methods with application to geothermal reservoir models. *Int. J. Num. Methods Fluids* (in press).

Gary, J. & Kassoy, D. R. 1981 *J. Comp. Phys.* **40**, 120.

Joseph, D. D. 1976 *Stability of Fluid Motions II.* Springer.

Kassoy, D. R. & Zebib, A. 1975 *Phys. Fluids* **18**, 1649.

Lindberg, B. 1976 *Dep. Comp. Sci., Univ. Illinois, Urbana, Rep.* UIUCDCS-R-76-820.

Morland, L., Zebib, A. & Kassoy, D. R. 1977 *Phys. Fluids* **20**, 1255.

Palm, E., Weber, J. E. & Kvernvold, O. 1972 *J. Fluid Mech.* **54**, 153.

Straus, J. M. & Schubert, G. 1977 *J. Fluid Mech.* **82**, 325.

Straus, J. M. & Schubert, G. 1978 *J. Fluid Mech.* **87**, 385.

Swarztrauber, P. & Sweet, R. 1975 *Nat. Center Atmos. Res. Tech. Note.* TN/IA-109.

Torrance, K. E. & Turcotte, D. L. 1971 *J. Fluid Mech.* **47**, 113.

Wooding, R. 1957 *J. Fluid Mech.* **2**, 273.